Journal of Material Cycles and Waste Management (2023) 25:2205–2221
https://doi.org/10.1007/s10163-023-01673-0

ORIGINAL ARTICLE

Recycling of printed circuit board e-wastes: a combined study of pyrolysis characteristics, kinetics and evolved gas analyses at various particle sizes

Havva Hande Cebeci[1] · Korkut Açıkalın[2] · Aysel Kantürk Figen[1,3]

Received: 24 November 2022 / Accepted: 11 April 2023 / Published online: 19 April 2023

Abstract

The current study aimed to determine the characteristics and kinetic parameters for the pyrolysis of printed circuit board (PCB) wastes including the analysis of evolved gases during the processes at different particle sizes. First, PCB wastes were examined using SEM–EDS, SEM-Mapping and FTIR to gain a better understanding of their structures. Then, non-isothermal TG-FTIR analyses of PCB wastes were conducted from ambient temperature to 800 °C under N_2 atmosphere. The thermal decomposition of PCB wastes occurred in four stages. The second stage was determined as the main pyrolysis stage. The average apparent activation energies (E_a) of main pyrolysis stage calculated using the isoconversional methods (Friedman, Flynn–Wall–Ozawa, Kissinger–Akahira–Sunose and Starink) were in the ranges of 205–240, 144–158 and 147–161 kJ mol^{-1} ranges for the studied particle sizes of PCB-2 (180 µm–1.18 mm), PCB-3 (90–180 µm) and PCB-4 (63–90 µm), respectively, which pointed out an effect of particle size on E_a value conversely to a previously reported literature study. Moreover, Coats-Redfern and Criado methods confirmed each other and revealed the reaction mechanism of main pyrolysis stage as F2-2.5. Based on the evolved gas analyses, the most common emission of PCB wastes was CO_2 associated with plastic, brominated compounds, polycarbonate, and epoxy resins decomposition.

Keywords Printed circuit board · Pyrolysis characteristics · Pyrolysis kinetics · Evolved gas analysis · TG-FTIR

Introduction

Electronic waste (e-wastes) has become one of the most significant environmental pollution causal in recent years due to dramatic increase in the use of electronic and electronic devices and a very short lifespan of them [1, 2]. The growth rate of e-wastes is reported to be 3% up to 5% per year which is one of the fastest growing waste streams in the world [3]. The annual generated global e-waste amount is predicted to be 20–50 million tonnes. In particular, printed circuit boards (PCB) wastes, which contain metallic and non-metallic fractions, constitute an important part of e-wastes [4]. PCB wastes are considered as an environmental pollutant due to their epoxy resin and phenolic based polymer contents while they are also valuable secondary resources because of metallic content in their complex structure [5, 6]. Recycling and recovering processes offer an opportunity to transform e-waste into valuable chemicals and materials as feedstocks such as metals [7], oil [8] and pyrolytic carbon [9] for energy storage applications [10], fuel production and electronic industry [8].

Pyrolysis is among the most attractive recycling options since it has the potential of recycling all the valuable materials in waste PCBs, especially for the organic constituents. Pyrolysis can be defined as the thermal decomposition of organic constituents in the absence of reactive gases such as oxygen, yielding solid (char), liquid (pyrolytic oil) and gaseous products that can be utilized as fuel and/or chemicals. The liquid and gaseous products of pyrolysis may serve for energetic purposes whereas the solid product may be evaluated for metal recovery and glass fibre reuse [11, 12]. Evangelopoulos et al. [13], reported that thermal degradation of non-metallic PCB

✉ Aysel Kantürk Figen
akanturk@yildiz.edu.tr

[1] Department of Chemical Engineering, Yıldız Technical University, 34220 Istanbul, Turkey

[2] Department of Energy Systems Engineering, Yalova University, 77200 Yalova, Turkey

[3] Clean Energy Technologies Institute, Yıldız Technical University, 34220 Istanbul, Turkey

wastes occurred in two regions and was more complex than a single plastic component. Moreover, Liu et al.[11], studied the pyrolysis of printed circuit boards in the absence and presence of copper metal. It was reported that metal presence resulted in shorter reaction time and lower activation energy.

Pyrolysis characteristics and kinetics of PCB wastes are required to design, operate and optimize thermochemical conversion units such as pyrolysis reactors. Thermogravimetric analysis (TGA) is a relatively easy and straightforward technique to obtain mass loss data from which kinetic parameters of pyrolysis can be calculated and pyrolysis behaviours can be determined [14]. For instance, Quan et al. [15] investigated the pyrolysis of large PCB waste particles using specially designed laboratory-scale thermobalance (Macro-TG) and results showed that large particle has a pyrolysis reaction retardancy compared to powder one. Generally, model-fitting and model-free (isoconversional) kinetic methods are the commonly used tools to calculate kinetic parameters from the data provided by TGA. Kinetic parameters calculated from model-free methods are considered more consistent and reliable due to the absence of assumptions made in model-fitting methods [16–18]. However, model-free kinetic methods do not provide information about the pyrolysis mechanism. Master plot methods, such as Criado method, can be utilized to determine the appropriate pyrolysis mechanism as well as the model-fitting methods [19].

The literature review revealed that the pyrolysis kinetics and characteristics of PCB wastes were studied by separating their parts such as metal, capacitor, battery etc. in most of the available studies. In this sense, there are limited number of studies on the pyrolysis kinetics and characteristics of PCB wastes which are not separated from their metals, capacitors, batteries etc. In addition to that, very limited part of these studies were focussed on examining the effects of particle size. Moreover, up-to-date studies are also needed as PCB production methods and raw materials may change due to rapidly developing technology and renewed regulations. The present study was undertaken to fulfil the above mentioned lacks by examining the pyrolysis characteristics, kinetics and evolved gas analyses of current PCB wastes at various particle sizes so that necessary information to design, operate and optimize the pyrolysis processes of PCB wastes can be provided. It should also be mentioned that, to the best of the authors' knowledge, present study is the first study that applied Criado's $Z(\alpha)/Z(0.5)$ master plot method to examine the pyrolysis mechanism of PCB wastes.

Materials and methods

Materials

In this study, thermal recycling of PCB waste was targeted by applying pyrolysis process. PCB wastes were provided by Proses Rafinasyon ve Metal Geri Kazanım Makina Sistemleri Company, Turkey. Electronic circuit boards known as motherboards were removed from the waste computers, and then, were shredded together with their components such as resistance, relay, capacitor, transistor, heat sink, chip lines and processors.

First, sieve analysis was performed to determine the particle size distribution of PCB waste using vibratory sieve machine (Fritsch, Analysette 3 Spartan). The sieves of mesh numbers 16, 80, 170 and 230 (corresponding diameters as 1.18 mm, 180 µm, 90 µm and 63 µm, respectively) were utilized. With respect to sieve analysis, four kinds of waste at different particle sizes were classified and named as PCB-1, PCB-2, PCB-3 and PCB-4 (SUBTable 1), and then, stored for further use. SUBTable 1 shows the results obtained from the sieve analyses performed on PCB wastes. After the waste particles passed through a set of sieves having the sizes of 1.18 mm, 180 µm, 90 µm and 63 µm, the retained masses were measured and the percentages of passing wastes were calculated. Evidently, fine and coarse wastes having different particle sizes were obtained. The calculated values clearly indicated that most of the PCB wastes (82%) collected were on the second sieve (-180 µm) representing the PCB-2 sample. Lesser fractions of wastes were collected on the last two bottom sieves (i.e. PCB-3 and PCB-4). The PCB-1 sample was not included in further studies since it was obviously the most heterogeneous fraction and consisted irregularly largest particles which were highly expected to result in completely different heat and mass transfer characteristics during the thermogravimetric pyrolysis process.

Physicochemical analyses including particle size distribution, FTIR, SEM–EDS and SEM-Mapping were conducted all fractions of PCB wastes. Especially, SEM–EDS and SEM-Mapping were performed for raw PCB wastes. The FTIR spectrums of the samples were recorded in air at room temperature by FTIR spectrophotometer (Perkin Elmer Spectrum One) equipped with Attenuated Total Reflectance (ATR) in the spectral range of 4000 to 650 cm^{-1}, and the resolution was 4 cm^{-1}. The morphologies, elemental analysis and mapping of the particles were examined using a scanning electron microscopy (SEM, ZEISS EVO LS10) equipped with energy dispersive spectroscopy (EDS). A Shimadzu ICPE 9000 spectrometer was used for the ICP-OES analysis.

Moreover, carbon, hydrogen and nitrogen elements were analysed simultaneously using a small amount (~2 mg) of sample with LECO, CHNS-932 elemental analyser. The proximate analyses of the samples were performed in accordance with ASTM E1131-03 standard. The results of proximate and ultimate analyses are presented in Table 1.

Thermogravimetric analysis (TGA)

The pyrolysis of PCB wastes was studied thermogravimetrically to collect the data on which the determination of pyrolysis characteristics and the calculation of kinetic parameters were performed. The non-isothermal TGA measurements were conducted from ambient temperature to 800 °C at the heating rates of 5, 10 and 20 °C min^{-1} under 200 ml min^{-1} flowrate of N_2 gas using SII6000 EXSTAR TG/DTA 6300 (Seiko Instruments, Japan) model thermogravimetric analyser. 10 ± 0.2 mg of sample, settled in platinum crucible, was used in each experiment. The N_2 gas used in the experiments had a purity ≥ 99.999%.

Kinetic theory

Pyrolysis of PCB waste is a solid-state thermal decomposition process. It is generally a complex process, but can be represented by the following simple reaction scheme:

$$A(\text{solid}) \rightarrow B(\text{solid}) + C(\text{volatile}) \quad (1)$$

The rate of pyrolysis process can be given by the following equation:

$$\frac{d\alpha}{dt} = k(T)f(\alpha) \quad (2)$$

where α, $k(T)$ and $f(\alpha)$ are degree of conversion, reaction rate constant and reaction model (or reaction mechanism), respectively.

Degree of conversion, or the fraction of pyrolyzed reactant (i.e. PCB waste) can be calculated by the initial mass of reactant at the beginning (m_o), the mass of reactant at time t (m_t) and the mass of reactant at the end of event of interest (m_f) as follows:

$$\alpha = \frac{(m_0 - m_t)}{(m_0 - m_f)} \quad (3)$$

In the case of thermally stimulated processes, reaction rate constant is expressed by Arrhenius equation ($k(T) = Ae^{-\frac{E_a}{RT}}$). Moreover, $dt = dT/\beta$ equation is applied for non-isothermal cases. Then, making some rearrangements, Eq. (4) can be obtained as follows:

$$\frac{d\alpha}{f(\alpha)} = \frac{A}{\beta}e^{-\frac{E_a}{RT}}dT \quad (4)$$

where A, β, E_a, R and T are pre-exponential factor ($time^{-1}$), heating rate ($K\ time^{-1}$), apparent activation energy ($J\ mol^{-1}$), gas constant (8.314 J mol^{-1} K^{-1}) and temperature (K), respectively.

Equation (4) is the differential form of fundamental equation that can be used to calculate kinetic parameters from non-isothermal TGA data. Integrating Eq. (4), the following equation is obtained [20]:

$$g(\alpha) = \int_0^{\alpha} \frac{d\alpha}{f(\alpha)} = \int_0^{T} \frac{A}{\beta}e^{-\frac{E_a}{RT}}dT = \frac{AE_a}{\beta R}p(x) \quad (5)$$

Here, $g(\alpha)$ is the integral form of the reaction model and $x = E_a/RT$. The temperature integral, $p(x)$, has no exact analytical solution. However, several approximation methods were suggested to solve the temperature integral which resulted in a large variety of approximate integral methods.

Coats-Redfern (CR) method

CR method is a model-fitting integral method. CR equation [21] is given below:

$$\ln\left(\frac{g(\alpha)}{T^2}\right) = \ln\left(\frac{AR}{\beta E_a}\right) - \frac{E_a}{RT} \quad (6)$$

As it can be seen from Eq. (6), the calculation results depend on the selection of kinetic mechanism that specifies $g(\alpha)$. Some reaction mechanisms required to describe solid-state thermal decomposition and their corresponding $g(\alpha)$ expressions can be found elsewhere [22]. In CR method, a straight line should be obtained by plotting $\ln\left(\frac{g(\alpha)}{T^2}\right)$ versus T^{-1}. Thus, several $\ln\left(\frac{g(\alpha)}{T^2}\right)$ versus T^{-1} graphs can be plotted for different reaction mechanisms, and these plots can be fitted to linear regression equations. Then, the reaction

Table 1 The results of proximate and ultimate analyses of PCB waste

Sample	C %	H %	N %	Moisture %	Volatiles %	Fixed carbon %	Ash %
PCB-2	24.60	2.36	0.74	0.45	32.29	6.80	60.46
PCB-3	20.00	1.91	0.5	0.39	20.52	3.63	75.46
PCB-4	12.90	1.29	< 0.1	0.27	17.25	1.95	80.53

mechanism can be revealed by determining the highest R^2 (regression coefficient) of fitted linear regression equations among the attempted reaction mechanisms.

Friedman (FR) method

FR method is an isoconversional differential method obtained by taking the natural logarithm of Eq. (4) as given below [23]:

$$\ln\left(\beta\frac{\mathrm{d}\alpha}{\mathrm{d}T}\right) = \ln(Af(\alpha)) - \frac{E_\mathrm{a}}{RT} \tag{7}$$

In FR method (Eq. 7), $\ln\left(\beta\frac{\mathrm{d}\alpha}{\mathrm{d}T}\right)$ versus T^{-1} graph is plotted at different heating rates for constant conversion values to obtain straight lines. Then, activation energy (E_a) values can be calculated from the slopes ($-\frac{E_\mathrm{a}}{R}$).

Flynn–Wall–Ozawa (FWO) method

FWO method is an isoconversional integral method, and utilizes the following equation [24]:

$$ln(\beta) = \ln\left(\frac{AE_\mathrm{a}}{Rg(\alpha)}\right) - 5.331 - 1.052\frac{E_\mathrm{a}}{RT} \tag{8}$$

FWO method requires the plotting of $\ln(\beta)$ versus T^{-1} graph at different heating rates for given values of conversion that should give straight lines. Then, the E_a can be calculated from the slopes ($-1.052\frac{E_\mathrm{a}}{R}$) of these straight lines.

Kissinger–Akahira–Sunose (KAS) method

KAS method is an isoconversional integral method whose equation is given as follows [25]:

$$\ln\left(\frac{\beta}{T^2}\right) = \ln\left(\frac{AR}{E_\mathrm{a}g(\alpha)}\right) - \frac{E_\mathrm{a}}{RT} \tag{9}$$

In this method, $\ln\left(\frac{\beta}{T^2}\right)$ versus T^{-1} graph is plotted at different heating rates for given values of conversion to yield straight lines. Then, E_a can be calculated from the slopes ($-\frac{E_\mathrm{a}}{R}$) of straight lines.

Starink (ST) method

Starink method is also an isoconversional integral method, and is expressed as follows [26]:

$$\ln\left(\frac{\beta}{T^{1.92}}\right) = C_\mathrm{s} - 1.0008\frac{E_\mathrm{a}}{RT} \tag{10}$$

Here, C_s is constant. In Starink method, $\ln\left(\frac{\beta}{T^{1.92}}\right)$ versus T^{-1} graph is plotted at different heating rates for given values of conversion to yield straight lines. Then, E_a can be calculated from the slope ($-1.0008\frac{E_\mathrm{a}}{R}$) of mentioned straight lines.

Criado method

Criado method can be utilized to determine the reaction mechanism of pyrolysis process, and is given by the following equation [27]:

$$\frac{Z(\alpha)}{Z(0.5)} = \frac{f(\alpha)g(\alpha)}{f(0.5)g(0.5)} = \left(\frac{T_\alpha}{T_{0.5}}\right)^2\frac{(\mathrm{d}\alpha/\mathrm{d}t)_\alpha}{(\mathrm{d}\alpha/\mathrm{d}t)_{0.5}} \tag{11}$$

where 0.5 refers to the degree of conversion, thus, $f(0.5)$, $g(0.5)$, $T_{0.5}$ and $(\mathrm{d}\alpha/\mathrm{d}t)_{0.5}$ correspond to the values of $f(\alpha)$, $g(\alpha)$, T and $\mathrm{d}\alpha/\mathrm{d}t$ at $\alpha = 0.5$, respectively. In Eq. (11), $(f(\alpha)g(\alpha))/(f(0.5)g(0.5))$ represents the reduced theoretical curve whereas the far right hand side of Eq. (11) associates with reduced rate. The reduced theoretical curve is characteristic of reaction mechanism, and can be calculated using the algebraic expressions of $f(\alpha)$ and $g(\alpha)$. On the other hand, reduced rate curve can be directly calculated from the experimental data. Then, the obtained reduced curves are simply compared for best available match to determine the reaction mechanism that describes the pyrolysis process.

Evolved gas analysis

Pyrolysis gas products, evolved during the pyrolysis experiments, were analysed by gas-phase FTIR spectroscopy. The TG–FTIR system composed of SII6000 Exstar TG/DTA 6300 Instrument and Perkin Elmer Spectrum 100 Fourier Transform Infrared Spectrometer. The transfer line used to connect TGA and FTIR equipments was maintained at 200 °C. The FTIR real time spectra were collected at 4 cm^{-1} resolution, co-adding 16 scans per spectrum.

Liquid phase analysis

In addition to evolved gas analysis, liquid phase analysis was also performed to identify and quantify the content. Thermal decomposition under nitrogen atmosphere-pyrolysis experiments were performed under nitrogen atmosphere in a semi-batch type reactor (316 L stainless steel) especially designed for the pyrolysis process. 15 g of PCB-2 was placed to the reactor and the reactor was degassed with N_2 gas for 15 min, and then heated up to 500 °C at 20 °C/min ramp and under nitrogen flow rate of 0.01 L/min. During this heating process, volatile gases were transferred to the two-stage cooling chamber where some of them was recovered through condensation. At the end of the pyrolysis experiments, the system was allowed to cool down to the room temperature. The pyrolysis liquid was collected from the pyrolysis reactor, and

Table 2 Properties of main pyrolysis stage of PCB wastes for studied heating rates and particle sizes

Property	Heating rate/°C min^{-1}								
	5			10			20		
	PCB-2	PCB-3	PCB-4	PCB-2	PCB-3	PCB-4	PCB-2	PCB-3	PCB-4
T_i/°C	289	285	288	295	298	298	308	311	315
T_f/°C	374	368	366	383	382	381	388	397	391
T_{max}/°C	324	326	317	338	341	330	347	355	347
W_{max}/% min^{-1}	1.99	1.32	1.30	4.80	3.03	2.63	9.25	6.59	5.24
Mass loss/%	22.66	13.12	10.49	23.47	13.40	10.60	21.49	15.27	10.82

then subjected to GC–MS analysis (GCMS-QP2010 Ultra, SHIMADZU) for detecting the structures and their content. SUB Table2 shows the main compositions of the pyrolysis liquid and the composition fraction of the liquid products calculated from the GC peak area.

Results and discussion

Physicochemical analyses

To obtain information about surface morphology, semi-quantitative analysis and elemental distribution of raw PCB and PCB waste fractions were investigated using SEM–EDS and SEM-Mapping analyses. Raw PCB waste was found to be contained 31% of Cu, 21.4% Fe, 18.2% Sn, 12.1% Si, 6.8% Ca, 5.9% Al, 1.9% Pd and 2.4% minor elements (Pb, Cr, Br, Mg, Na, Ti, Mn, Sb, Co). The SEM images of different fractions of the PCB wastes are shown in SUBFIG 1. SEM images showed various content at different shapes. Striped structures confirmed the glass fibre content of e-waste fraction while spherical structures indicated the presence of metallic content. The PCB samples at each fraction demonstrated the presence of oxygen, silicon and calcium as major constituents. The presence of Fe as another major element in spherical structures of PCB-2 and PCB-4 was also noticed while Sn was observed as another major constituent of PCB-3 fraction. According to the ICP-OES analysis, the Cu (10.52%), Al (1.5%), Fe (2.23%), Sn (3.34%) and Zn (3.72%) were determined as major elements with high amounts compared to the minor elements such as Pb (0.2%) and Pd (0.0073%) in the PCB-2 fraction whose pyrolysis characteristics were further investigated.

To obtain information about functional groups, and therefore, about the polymers present in the PCB wastes at different particle sizes, FTIR-ATR analyses were carried out. According to the SUBFIG 2, 3500–3600 cm^{-1} spectral range was attributed to the O–H band due to the water content. The weak peak at 2900 cm^{-1} was associated with aromatic asymmetric and symmetrical C–H stress vibrations. The peak at 1720 cm^{-1} might be due to carbonyl stretch vibrations of carboxylic acid esters. The peak at approx. 1228 cm^{-1} showed bending vibrations aliphatic C–O or C–H. The band between 1166 and 838 cm^{-1} indicates the existence of epoxy group [28]. According to the FTIR spectra, the polymer fraction of the e-waste was found as ester resins.

Proximate and ultimate analyses results are listed in Table 1. The moisture content of PCB-4 was slightly lower than the other fractions. Moisture contents were not high enough to effect the pyrolysis and combustion characteristics associated with fuel quality. Thus, pre-drying of samples are not required prior to the relevant processes. The highest volatile matter, fixed carbon and hydrogen contents belonged to the PCB-2 fraction, and, thus, PCB-2 fraction was found more appropriate as pyrolysis feedstock. Ultimate analysis of e-waste revealed C, H and N contents. These results are consistent with the ultimate analysis results of the study performed by Evangelopoulos et al. [13].

Pyrolysis characteristics of PCB wastes

Thermogravimetric analyses of PCB wastes at three different particle sizes (PCB-2, PCB-3 and PCB-4) were performed from ambient temperature to 800 °C at three different heating rates (5, 10 and 20 °C min^{-1}) under 200 ml min^{-1} N_2 flowrate to generate TG (thermogravimetric) and DTG (derivative thermogravimetric) curves. The generated TG and DTG curves are presented in Fig. 1. When substances are subjected to pyrolysis process thermogravimetrically, characteristic TG/DTG curves are generated due to the decomposition of the components in their structures at different temperature ranges and decomposition rates. These curves host important information that can be used in the design and optimization of the related pyrolysis processes as well as the determination of pyrolysis behaviours of particular substances. In addition, recognizing the components of the substance undergoing pyrolysis process makes it easy to understand and interpret its pyrolysis characteristics, and may even form a basis for this progress. From this point of view, it is important to know that PCB is essentially a heterogeneous substance consisting of organic, metal and non-metal parts. Organic fraction of PCB is mainly epoxy

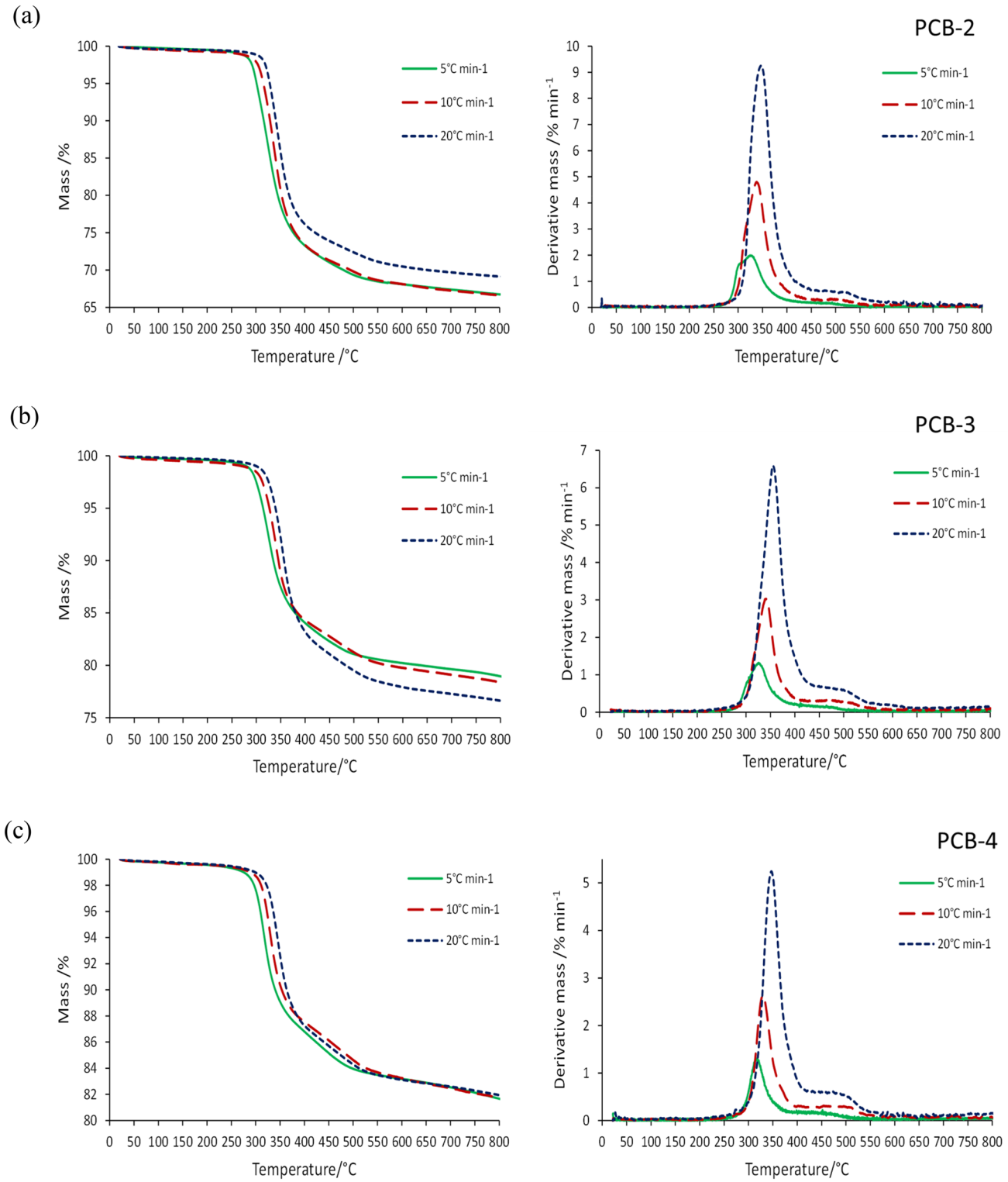

Fig. 1 TG and DTG curves of PCB wastes for studied particle sizes **a** PCB-2, **b** PCB-3, **c** PCB-4

resin filled with brominated fire retardants to decrease flammability. Main metal available in PCBs is copper to provide electrical conductivity whereas the main non-metals are glass fibres (SiO_2, CaO), fillers in epoxy resin, ceramics and insulators [29]. So, considering the components of the PCB, it is known that the organic fraction decomposes during the

pyrolysis process while metals, fillers, glasses, etc. generally remain unchanged [15]. These information should be kept in mind as they constitute the basis for understanding and interpreting the pyrolysis behaviour of PCB wastes.

Pyrolysis stages can be determined by examining the slope changes on the TG curve and the peak structure of DTG curve. For this purpose, the TG and DTG curves obtained for PCB-3 particle size at 10 °C min^{-1} heating rate (Fig. 1b) were examined, and it was observed that PCB pyrolysis process occurred in four different decomposition stages. The first stage took place between ambient temperature and 298 °C with a mass loss of approx. 1.45%. The rate of decomposition in this stage was considerably low, and the highest value was obtained as 0.34%/min at the final temperature of the stage. The mass loss of first stage can mainly be attributed to removal of water and CO_2 [30]. Water and CO_2 content were also confirmed by FTIR spectra of PCB samples (SUBFIG 2). Following the first stage, the decomposition rate started to increase considerably indicating that the active pyrolysis of PCB waste was initiated at 298 °C. As it can be observed from the DTG curve, there existed two overlapping decomposition stages between 298 and 561 °C due to the turning point at 382 °C which separated the mentioned temperature range into two stages that were named as second and third stages. A similar DTG curve was also observed by Sun et al. [18] for a similar temperature range with a turning point at around 430 °C. The second decomposition stage of PCB wastes appeared between 298 and 382 °C with by far the highest mass loss (13.40%) and the highest mass loss rate (3.03% min^{-1}) among the four decomposition stages. For this reason, the second decomposition stage was denoted as main pyrolysis stage. On the other hand, the third decomposition stage existed between 382 and 561 °C, and yielded a mass loss of 5.06%. The highest mass loss rate observed in third stage was 0.32% min^{-1}. It is reported that the thermal decomposition of brominated epoxy resins may consist of two independent reactions that are thermal decomposition of brominated and non-brominated compounds, and, these generally may overlap partially in some temperature ranges. In addition to that, it is confirmed that the brominated compounds are thermally less stable than the non-brominated compounds in brominated epoxy resins [11]. Moreover, Kim et al. [31] reported that brominated epoxy resin decomposed between 250 and 350 °C whereas non-brominated epoxy resin decomposed between 250 and 500 °C at slower decomposition rates compared to brominated epoxy resin. Based on these important information, second and third stages of PCB wastes can mainly be linked to the decomposition of brominated and non-brominated epoxy resin, respectively. The fourth and final decomposition stage of PCB was between 561 and 800 °C with a mass loss of 1.70%. The mass loss rates observed in fourth stage, which can be denoted as char stabilization stage, were very low compared to the previous stages, and the highest mass loss rate was determined as 0.11% min^{-1} at the initial temperature of the stage. The remaining residue at the end of the whole pyrolysis process was read as 78.37%.

The characteristic properties of main pyrolysis stage of PCB wastes, namely, T_i (starting temperature), T_f (ending temperature), T_{max} (the temperature at which maximum mass loss rate occurred) and W_{max} (maximum mass loss rate) were determined for all studied heating rates and particle sizes since calculation of kinetic parameters for main pyrolysis stage was another aim of the present study. The results are presented in Table 2.

It can be observed from Table 2 that increasing the heating rate yielded an increase in all characteristic temperatures (T_i, T_f and T_{max}) for all studied particle sizes. A temperature difference occurs between the surface of the PCB particle and the inner side of the PCB particle while the PCB sample is heated during the pyrolysis process. The higher the heating rate, the greater the temperature difference between the surface and the inner side of the PCB particles. Thus, pyrolysis reactions within the particle are completed later than those at the particle surface. This causes the characteristic temperatures to increase, leading the TG and DTG curves to shift to higher temperatures. It was also noted by Gao et al. [32] that escape of pyrolysis products could be restrained by higher surface temperature and lower inner temperature causing a decrease in the degree of pyrolysis reaction. Another interpretation was stated by Alenezi and Al-Fadhli [12] indicating the longer time requirement of nitrogen gas to reach thermal equilibrium with the sample due to the heat transfer limitations since large amount of instantaneous thermal energy is provided at higher heating rates. The shifting of TG/DTG curves to higher temperatures with increasing heating rate was also observed by many other researchers [11, 12, 15, 32–35]. The W_{max} value increased significantly with increasing heating rate for all studied particle sizes. This was an expected outcome since the energy input to the system was increased to provide higher heating rates. The highest increase in W_{max} by increasing the heating rate was observed at the largest particle size studied. As the particle size got smaller, the increase in W_{max} value decreased. This shows the effect of studied particle size on pyrolysis characteristics, and can be attributed to the decrease of mass transfer limitations with increasing particle size. It can be said that the mass loss remained roughly constant with increasing heating rate for all studied particle sizes. This indicated that the time required to complete the mass loss can be achieved at all studied heating rates.

The effect of particle size on pyrolysis characteristics of PCB wastes was also investigated during the present study. As evidenced by Table 2, it can be said that T_i value did not

change significantly and remained almost constant with the increasing particle size for heating rates studied. Quan et al. [15] also stated the same finding, that is, the particle size did not have significant effect on the initial reaction temperature value. Likewise, the increasing particle size did not have a significant influence on T_f at all studied heating rates since the changes observed in T_f values were notably limited. On the other hand, T_{max} values first increased slightly with increasing particle size, and then, remained almost constant with further increase of particle size. All these findings indicated that, on the contrary to heating rate, particle size was not significantly effective on the characteristic temperatures within the studied ranges. Besides, W_{max} value increased with increasing particle size at all studied heating rates but the highest increase was obtained at 20 °C min^{-1} heating rate. This situation was expected since the highest energy input to the pyrolysis system per unit time was provided at 20 °C min^{-1}. Finally, mass loss was significantly affected by the change in particle size, and increased with increasing particle size at all heating rates studied. This implies the positive effect of higher particle sizes on mass loss at studied ranges possibly by favouring the mass transfer.

Calculation of kinetic parameters

FR, FWO, KAS and ST methods were chosen as the kinetic methods to calculate the activation energy values of main pyrolysis stage of PCB wastes since these methods are commonly used isoconversional methods and are among the kinetic methods stated by ICTAC (International Confederation for Thermal Analysis and Calorimetry). Since only the activation energies can be calculated with isoconversional methods, CR and Criado's master plot methods were also used to determine the reaction mechanism. The reason for choosing more than one method to determine the reaction mechanism and activation energy was to determine the accuracy and reliability of the calculations.

In CR method, according to Eq. (6), $\ln\left(\frac{g(\alpha)}{T^2}\right)$ versus T^{-1} graphs were plotted using the $g(\alpha)$ expressions of 27 different reaction mechanisms given in [22]. The selection of appropriate reaction mechanism was based on the determination of the highest regression coefficient (R^2) value among the attempted reaction mechanisms since $\ln\left(\frac{g(\alpha)}{T^2}\right)$ versus T^{-1} plot should give a straight line, in other words, R^2 value of the fitted equation should converge to 1. For this reason, all of the plotted $\ln\left(\frac{g(\alpha)}{T^2}\right)$ versus T^{-1} graphs were fitted to linear regression equations, and the R^2 value of these fitted equations were determined. The results obtained for all studied heating rates and particle sizes are presented in Table 3. As it can be seen from Table 3, the highest R^2 values (0.9401–0.9678) were obtained for F2 type order of reaction model for all the studied particle sizes and heating rates indicating that the reaction mechanism was independent of studied heating rates and particle sizes. The order of reaction (n) was roughly found 2 as stated above, but to find the exact value of the n and to calculate the kinetic parameters more precisely, R^2-n graphs (SUBFIG 3) were generated by choosing various n values around 2. The exact (or most appropriate) n, i.e. the n value providing the highest R^2 value, was determined from the generated R^2—n curves. To determine the n value that has the highest R^2, the R^2-n plots were fitted to second order polynomial equations.

As it can be seen from SUBFIG 3, the R^2 values of the fitted polynomial equations were ≥ 0.9944 indicating a reliable fitting. The fitted polynomial equations were differentiated to calculate the n value ensuring the highest R^2, since this requires the slope of fitted polynomial equations to be zero. Then, solving the differential equations for zero, the exact n values were calculated for all studied heating rates and particle sizes. The reaction orders calculated using CR method are shown in Table 4. To check the validity of the reaction mechanism determined by the CR method, it was also aimed to determine the reaction mechanism using Criado method. For this purpose, based on Eq. (11), reduced theoretical and reduced rate curves were created for all studied heating rates and particle sizes. The relevant plots are presented in Fig. 2. When Fig. 2 is examined carefully for PCB-2 (Fig. 2a–c) and PCB-3 (Fig. 2d–f), it can be seen that the reduced rate curves almost overlapped with the F2 theoretical curves for app. $0.25 \leq \alpha \leq 0.85$. When the same examination is made for PCB-4 (Fig. 2g–i), it appeared that the reduced rate curves almost completely overlapped with the theoretical curves of F2.5 over the range of app. $0.15 \leq \alpha \leq 0.85$. Comparing these results with the results of n obtained from CR method (Table 4), it can be said that CR and Criado methods agreed very well for PCB-2 and PCB-3 fractions, and agreed partially well for PCB-4 fraction. So, considering the results of CR and Criado methods together, it would be right to say that the reaction mechanism of main pyrolysis stage of PCB samples fit F2-2.5 type for studied heating rate and particle size ranges. It can be said that the reaction mechanism of the main pyrolysis stage of PCB wastes were correctly and reliably determined considering the fact that two different methods produced substantially overlapping results in terms of reaction mechanisms.

FR method was utilized to calculate E_a values of main pyrolysis stage of PCB wastes. Considering Eq. (7), $\ln\left(\beta\frac{d\alpha}{dT}\right)$ versus T^{-1} graphs of PCB wastes were plotted at the heating rate values of 5, 10 and 20 °C min^{-1} for 0.1–0.9 conversion range (Fig. 3a–c). Then, linear regression equations were fitted to plots, and the R^2 values of the fitted equations were determined. Finally, E_a values were calculated from the

Table 3 The R^2 values of fitted equations determined for main pyrolysis stage of PCB wastes using CR method for studied reaction mechanisms, particle sizes and heating rates

No	Code of reaction mechanism	R^2								
		Particle size								
		PCB-2			PCB-3			PCB-4		
		Heating rate/°C min^{-1}								
		5	10	20	5	10	20	5	10	20
1	F0	0.6979	0.7615	0.7618	0.7645	0.7828	0.7944	0.7271	0.7438	0.7556
2	F0.5	0.7842	0.8290	0.8284	0.8322	0.8472	0.8584	0.8020	0.8140	0.8280
3	F1	0.8699	0.8984	0.8967	0.8986	0.9119	0.9196	0.8797	0.8891	0.9012
4	F1.5	0.9202	0.9392	0.9459	0.9424	0.9552	0.9592	0.9350	0.9404	0.9496
5	F2	0.9401	0.9609	0.9633	0.9529	0.9670	0.9678	0.9534	0.9635	0.9654
6	F2.5	0.9317	0.9539	0.9587	0.9426	0.9582	0.9570	0.9489	0.9609	0.9598
7	F3	0.9166	0.9387	0.9452	0.9252	0.9422	0.9396	0.9362	0.9494	0.9467
8	F3.5	0.9015	0.9224	0.9299	0.9074	0.9253	0.9219	0.9224	0.9362	0.9326
9	F4	0.8884	0.9076	0.9156	0.8916	0.9101	0.9061	0.9099	0.9239	0.9199
10	D1	0.7161	0.7738	0.7727	0.7772	0.7938	0.8054	0.7409	0.7566	0.7677
11	D2	0.7633	0.8110	0.8182	0.8149	0.8294	0.8413	0.7820	0.7946	0.8073
12	D3	0.8245	0.8600	0.8586	0.8627	0.8758	0.8861	0.8367	0.8469	0.8602
13	D4	0.7846	0.8279	0.8263	0.8316	0.8455	0.8569	0.8008	0.8126	0.8256
14	D5	0.9136	0.9365	0.9355	0.9346	0.9465	0.9516	0.9239	0.9308	0.9394
15	A1.5	0.8626	0.8935	0.8923	0.8936	0.9078	0.9156	0.8741	0.8840	0.8968
16	A2	0.8548	0.8883	0.8877	0.8881	0.9034	0.9114	0.8681	0.8785	0.8921
17	A3	0.8370	0.8766	0.8775	0.8760	0.8937	0.9019	0.8548	0.8664	0.8817
18	A4	0.8162	0.8631	0.8659	0.8619	0.8825	0.8910	0.8397	0.8526	0.8699
19	B1[a]	0.6553	0.6783	0.6743	0.6806	0.6838	0.6817	0.6541	0.6591	0.6556
20	P2/3	0.7102	0.7698	0.7691	0.7731	0.7902	0.8018	0.7364	0.7524	0.7637
21	P2	0.6567	0.7339	0.7378	0.7361	0.7583	0.7697	0.6964	0.7154	0.7287
22	P3	0.6086	0.7022	0.7106	0.7032	0.7300	0.7410	0.6613	0.6828	0.6980
23	P4	0.5526	0.6655	0.6797	0.6649	0.6974	0.7075	0.6211	0.6456	0.6628
24	E1[b]	N/A	N/A	N/A	N/A	N/A	N/A	N/A	N/A	N/A
25	E2[b]	N/A	N/A	N/A	N/A	N/A	N/A	N/A	N/A	N/A
26	R2	0.7842	0.8290	0.8284	0.8322	0.8472	0.8584	0.8020	0.8140	0.8280
27	R3	0.8141	0.8529	0.8523	0.8555	0.8679	0.8802	0.8286	0.8394	0.8535

[a]B1 results were affected by the ln $(g(\alpha)/T^2)$ values which were "undefined" for $\alpha < 0.5$

[b]E1 and E2 were not applicable since ln $(g(\alpha)/T^2)$ values were "undefined" for $0.1 \leq \alpha \leq 0.9$

slopes of fitted equations. The fitted equations, their corresponding R^2 values and the calculated E_a values for all studied particle sizes are presented in Table 5. As it can be observed from Table 5, the average R^2 values of fitted equations for FR method were ≥ 0.9863 indicating a good linearity of the plots which is a sign of reliability since the method was expected to yield straight lines.

E_a values of main pyrolysis stage of PCB wastes were also calculated using FWO method. Taking Eq. (8) as the basis, ln(β) versus T^{-1} graphs of PCB wastes were plotted at studied heating rates (5, 10 and 20 °C min^{-1}) for the conversion values between 0.1 and 0.9 (Fig. 3d–f). Then, the procedure explained in above paragraph was followed. The fitted equations, their corresponding R^2 values and the calculated E_a values for all studied particle sizes using FWO method are demonstrated in Table 5. The average R^2 values of fitted equations for FWO method were ≥ 0.9941 (Table 4). This high value of average R^2 was interpreted as a sign of good linearity, and thus, reliability, since the method was anticipated to generate straight lines.

The calculation of E_a values for main pyrolysis stage of PCB wastes was also executed using KAS method. According to Eq. (9), $\ln\left(\frac{\beta}{T^2}\right)$ versus T^{-1} graphs were plotted at 5, 10 and 20 °C/min heating rates for the conversion range of 0.1–0.9 (Fig. 3g–i). Then, the procedure explained for FR method was followed. The fitted equations, their corresponding R^2 values and the calculated E_a values for all studied particle sizes using KAS method are shown in Table 5. The average R^2 values of fitted equations for KAS

Table 4 The reaction order (n) of main pyrolysis stage of PCB wastes calculated by CR method for all studied heating rates and particle sizes

β/°C min^{-1}	Fitted equation	R^2	n
PCB-2			
5	$y=-31131x+39.132$	0.9401	2.00
10	$y=-36088x+46.286$	0.9609	2.03
20	$y=-42102x+55.128$	0.9637	2.10
Avg			2.05
PCB-3			
5	$y=-32904x+42.125$	0.9531	1.95
10	$y=-37081x+47.743$	0.9670	1.98
20	$y=-35688x+44.024$	0.9681	1.92
Avg			1.95
PCB-4			
5	$y=-37900x+50.844$	0.9538	2.10
10	$y=-40211x+53.316$	0.9644	2.16
20	$y=-41476x+53.732$	0.9655	2.07
Avg			2.11

method were ≥ 0.9937 (Table 5) indicating the reliability of kinetic calculations performed using KAS method as explained in above methods.

The calculations to determine E_a values within the scope of ST method were carried out according to Eq. (10). Thus, $\ln\left(\frac{\beta}{T^{1.92}}\right)$ versus T^{-1} graphs were plotted at heating rates of 5, 10 and 20 °C min^{-1} for the conversion range of 0.1 to 0.9 (Fig. 3j–l). Then, the procedure explained for FR method was followed. The fitted equations, their corresponding R^2 values and the calculated E_a values for all studied particle sizes using ST method are given in Table 5. ST method yielded average R^2 values ≥ 0.9935 (Table 5) for fitted equations indicating the reliability of performed kinetic calculations as explained for other isoconversional methods (i.e. FR and FWO) above.

Table 5 was examined to determine whether the calculated average E_a values were coherent or not. The standard deviations for the average E_a values using isoconversional integral methods (i.e. FWO, KAS and ST) were calculated as 0.41, 1.46, and 1.29 kJ mol^{-1} for PCB-2, PCB-3 and PCB-4 particle sizes, respectively. These values revealed that the average E_a results obtained using isoconversional integral methods were highly consistent for all studied particle sizes. In fact, this was an expected outcome since these three methods differ slightly and essentially involve using equations of the same form: $\ln(\beta/T^B) = \text{Constant} - CE_a/(RT)$ where B and C are parameters introducing different type of temperature integral approximation [36]. However, the high consistency was important in terms of providing opportunity to check against computational errors. Thus, the calculated standard deviation values eliminated the existence of such errors for the applied isoconversional integral methods. On the other hand, FR method is an isoconversional differential method and is in the form of an equation different from the FWO, KAS and ST methods. Therefore, the comparison of FR with other isoconversional integral methods is meaningful in terms of obtaining information about the reliability of the calculated average E_a results. Since the average values obtained from the FWO, KAS and ST methods were very close, the average value of these three methods and the average E_a value obtained from the FR method were compared. According to the comparison, the FR method yielded 16.8%, 8.6% and 8.7% higher results than the isoconversional integral methods for the particle sizes PCB-2, PCB-3 and PCB-4, respectively. This finding was attributed to the different approaches and approximations used in the methods. Moreover, it is also known that FR's model suffer from an inherent error resulting from the rate of instant reaction ($d\alpha/dt$) values [12]. Thus, considering these information, it would be righteous to state that the average E_a results calculated using isoconversional methods were concordant with each other.

The results calculated using all types of isoconversional methods revealed the dependency of E_a to degree of conversion (α) (Fig. 4). For instance, having examined the results of isoconversional integral methods (Fig. 4), it was observed that increasing the degree of conversion caused a continuous increase in the E_a values of the main pyrolysis stage of PCB wastes for all studied particle sizes. Another result revealed by Fig. 4 is that the E_a-α graphs of the isoconversional integral methods were almost superimposable. This means that the high agreement observed for the average E_a results was also recognized for the conversion based activation energy (E_α) values. This situation can be explained by the interpretation made in above paragraph to explain the high consistency obtained for the average E_a results calculated using the isoconversional integral methods. As it can be seen from Fig. 4, the E_α values calculated using the FR method increased with the increasing degree of conversion, except for a few points of the particle sizes PCB-3 and PCB-4, similar to those observed in isoconversional integral methods. However, in most of the cases, the E_α values calculated using the FR method were higher than those calculated using isoconversional integral methods. The difference between the E_α values calculated using the FR method and the isoconversional integral methods can be attributed to the varying approaches utilized in these methods and the intrinsic error of the FR method as already mentioned in the discussion of average E_a results. In addition, the E_a-α relationship obtained in the present study, i.e. the increase of E_a with increasing α, coincides with the tendency observed for polymers and complex organic substances which is found consistent with the residual material becoming increasingly refractory [36].

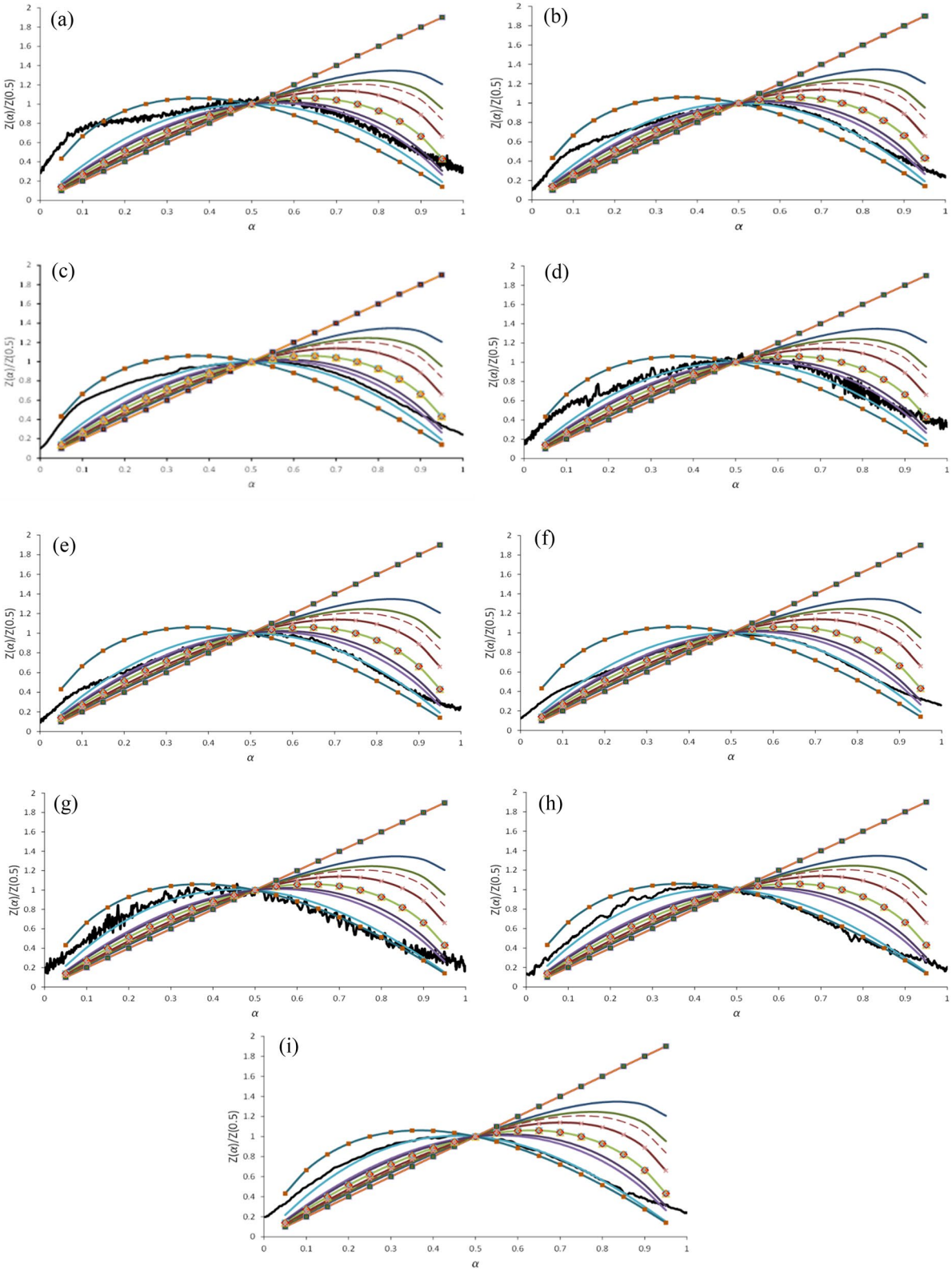

Fig. 2 Z(α)/Z(0.5) graphs plotted for Criado Method **a** PCB-2, 5 °C min^{-1}, **b** PCB-2, 10 °C min^{-1}, **c** PCB-2, 20 °C min^{-1}, **d** PCB-3, 5 °C min^{-1}, **e** PCB-3, 10 °C min^{-1}, **f** PCB-3, 20 °C min^{-1}, **g** PCB-4, 5 °C min^{-1}, **h** PCB-4, 10 °C min^{-1}, **i** PCB-4, 20 °C $min.^{-1}$

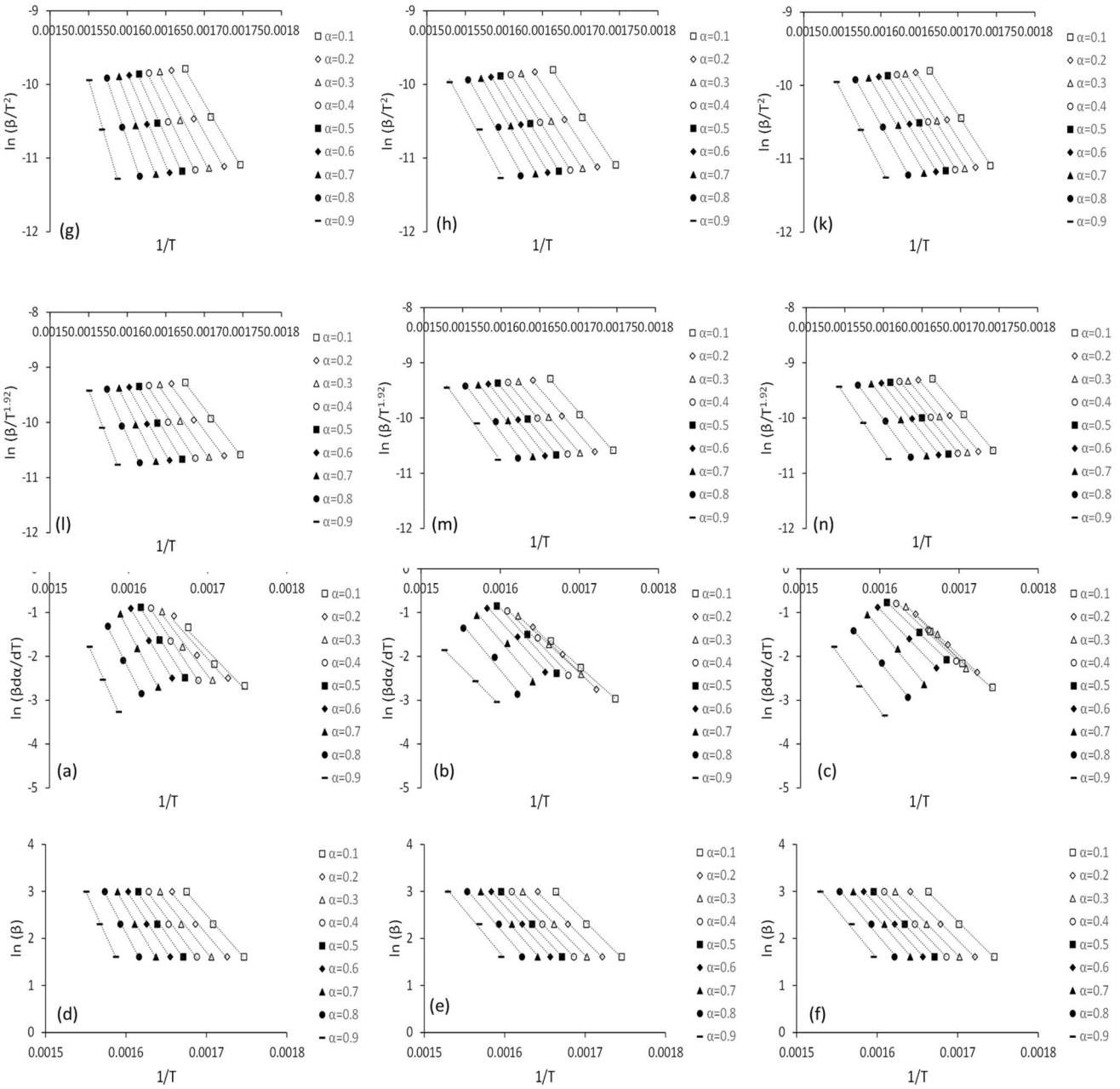

Fig. 3 Graphs of model-free kinetic methods plotted for **a** FR method, PCB-2, **b** FR method, PCB-3, **c** FR method, PCB-4, **d** FWO method, PCB-2, **e** FWO method, PCB-3, **f** FWO method, PCB-4, **g** KAS method, PCB-2, **h** KAS method, PCB-3, **i** KAS method, PCB-4, **j** ST method, PCB-2, **k** ST method, PCB-3, **l** ST method, PCB-4

Figure 5 demonstrates the change of average E_a with particle size for all studied kinetic methods. Having examined this figure, it can clearly be observed that the relationship between average E_a and particle size exposed a perfect match of trend for all studied isoconversional kinetic methods. The average E_a decreased significantly with the reduction of particle size from PCB-2 to PCB-3 (Fig. 5). When the particle size was further reduced and the value of PCB-4 was reached, the average E_a remained almost constant according to the results of isoconversional methods. So, from the general point of view, it can be concluded that the isoconversional kinetic methods utilized within the scope of present study yielded consistent average E_a-particle size relationships. As the particle size gets smaller, the temperature gradient within the pyrolyzed PCB particles gets lower. Thus, the temperature difference between the particle surface and inside decreases. This means that the pyrolysis reactions, both on the surface of the PCB particles and inside

Table 5 Kinetic parameters of main pyrolysis stage of PCB wastes calculated by FR, FWO, KAS and ST methods

α	PCB-2			PCB-3			PCB-4		
	R^2	Fitted equation	E_a/kJ mol^{-1}	R^2	Fitted equation	E_a/kJ mol^{-1}	R^2	Fitted equation	E_a/kJ mol^{-1}
FR method									
0.1	0.9643	$y=-18574x+29.701$	154.42	1.0000	$y=-16156x+25.232$	134.32	0.9964	$y=-16232x+25.547$	134.95
0.2	0.9435	$y=-20243x+32.354$	168.30	0.9989	$y=-17748x+27.807$	147.56	1.0000	$y=-17110x+27.113$	142.25
0.3	0.9837	$y=-24222x+38.736$	201.38	1.0000	$y=-16713x+26.041$	138.95	0.9916	$y=-18533x+29.431$	154.08
0.4	0.9974	$y=-27317x+43.552$	227.11	0.9918	$y=-19063x+29.745$	158.49	0.9920	$y=-17283x+27.250$	143.69
0.5	0.9976	$y=-28603x+45.297$	237.81	0.9900	$y=-20257x+31.513$	168.42	0.9994	$y=-17338x+27.132$	144.15
0.6	0.9991	$y=-30339x+47.703$	252.24	0.9922	$y=-19789x+30.463$	164.53	0.9996	$y=-18635x+28.891$	154.93
0.7	0.9990	$y=-34739x+54.168$	288.82	0.9790	$y=-21288x+32.420$	176.99	0.9970	$y=-22161x+34.079$	184.25
0.8	0.9961	$y=-35996x+55.303$	299.27	0.9748	$y=-21793x+32.555$	181.19	0.9983	$y=-22087x+33.208$	183.63
0.9	0.9959	$y=-40238x+60.589$	334.54	0.9999	$y=-17865x+25.462$	148.53	0.9908	$y=-24527x+36.010$	203.92
Avg	0.9863		240.43	0.9918		157.66	0.9961		160.65
FWO method									
0.1	0.9982	$y=-19403x+35.484$	153.34	0.9982	$y=-16982x+31.233$	134.21	0.9996	$y=-17629x+32.330$	139.32
0.2	0.9923	$y=-20098x+36.263$	158.84	0.9986	$y=-17249x+31.288$	136.32	0.9992	$y=-17834x+32.347$	140.94
0.3	0.9897	$y=-21517x+38.286$	170.05	0.9998	$y=-17395x+31.214$	137.47	0.9987	$y=-18003x+32.388$	142.28
0.4	0.9900	$y=-22899x+40.232$	180.97	0.9999	$y=-17974x+31.910$	142.05	0.9983	$y=-18294x+32.661$	144.58
0.5	0.9919	$y=-24600x+42.692$	194.42	0.9998	$y=-18313x+32.220$	144.73	0.9974	$y=-18378x+32.584$	145.24
0.6	0.9950	$y=-26391x+45.259$	208.57	0.9991	$y=-18871x+32.885$	149.14	0.9981	$y=-18656x+32.811$	147.44
0.7	0.9963	$y=-28950x+48.984$	228.79	0.9971	$y=-19565x+33.737$	154.62	0.9983	$y=-19323x+33.623$	152.71
0.8	0.9970	$y=-32504x+54.123$	256.88	0.9917	$y=-20150x+34.326$	159.25	0.9994	$y=-20176x+34.616$	159.45
0.9	0.9968	$y=-37511x+61.141$	296.45	0.9895	$y=-20717x+34.716$	163.73	0.9999	$y=-21690x+36.450$	171.42
Avg	0.9941		205.37	0.9971		146.84	0.9988		149.26
KAS method									
0.1	0.9980	$y=-18234x+20.743$	151.60	0.9980	$y=-15809x+16.484$	131.44	0.9995	$y=-16454x+17.578$	136.80
0.2	0.9914	$y=-18916x+21.499$	157.27	0.9990	$y=-15867x+16.181$	131.92	0.9991	$y=-16646x+17.572$	138.39
0.3	0.9885	$y=-20323x+23.502$	168.97	0.9998	$y=-16192x+16.414$	134.62	0.9985	$y=-16805x+17.597$	139.72
0.4	0.9889	$y=-21693x+25.429$	180.36	0.9999	$y=-16760x+17.092$	139.34	0.9980	$y=-17087x+17.856$	142.06
0.5	0.9911	$y=-23383x+27.870$	194.41	0.9998	$y=-17089x+17.385$	142.08	0.9970	$y=-17163x+17.765$	142.69
0.6	0.9945	$y=-25163x+30.420$	209.21	0.9990	$y=-17636x+18.033$	146.63	0.9977	$y=-17431x+17.977$	144.92
0.7	0.9960	$y=-27710x+34.125$	230.38	0.9966	$y=-18318x+18.867$	152.30	0.9980	$y=-18088x+18.771$	150.38
0.8	0.9980	$y=-31287x+39.304$	260.12	0.9905	$y=-18889x+19.433$	157.04	0.9993	$y=-18926x+19.741$	157.35
0.9	0.9966	$y=-36237x+46.227$	301.27	0.9880	$y=-19436x+19.791$	161.59	0.9999	$y=-20420x+21.542$	169.77
Avg	0.9937		205.95	0.9967		144.11	0.9986		146.90
ST method									
0.1	0.9980	$y=-18281x+21.333$	151.87	0.9980	$y=-15856x+17.074$	131.72	0.9995	$y=-16501x+18.169$	137.08
0.2	0.9914	$y=-18963x+22.090$	157.53	0.9984	$y=-16107x+17.102$	133.81	0.9991	$y=-16693x+18.163$	138.68
0.3	0.9885	$y=-20371x+24.094$	169.23	0.9998	$y=-16240x+17.006$	134.91	0.9985	$y=-16853x+18.189$	140.00
0.4	0.9889	$y=-21741x+26.021$	180.61	0.9999	$y=-16809x+17.685$	139.64	0.9980	$y=-17136x+18.449$	142.36
0.5	0.9912	$y=-23432x+28.463$	194.66	0.9998	$y=-17138x+17.978$	142.37	0.9970	$y=-17211x+18.357$	142.98
0.6	0.9945	$y=-25212x+31.013$	209.45	0.9990	$y=-17685x+18.627$	146.92	0.9978	$y=-17480x+18.570$	145.21
0.7	0.9960	$y=-27760x+34.719$	230.61	0.9966	$y=-18368x+19.462$	152.59	0.9980	$y=-18137x+19.365$	150.67
0.8	0.9968	$y=-31300x+39.836$	260.02	0.9906	$y=-18940x+20.028$	157.34	0.9993	$y=-18976x+20.336$	157.64
0.9	0.9966	$y=-36288x+46.824$	301.46	0.9881	$y=-19487x+20.388$	161.89	0.9999	$y=-20471x+22.139$	170.06
Avg	0.9935		206.16	0.9967		144.58	0.9986		147.19

the PCB particles, will take place at adjacent temperatures or times. In other words, distinctly higher temperatures or times will not be required to complete the pyrolysis reactions occurring inside the particle. So, that leads to reduced energy consumption to complete the pyrolysis reactions. The decrease in the average E_a value by decreasing the particle size from PCB-2 to PCB-3 can be explained in this manner. On the other hand, no significant change in the average E_a values was observed by further decreasing the particle size from PCB-3 to PCB-4, and the average E_a value remained almost constant. This indicates that the decrease in particle size induced a considerably lower change in the temperature gradient which did not cause the above mentioned effect. Therefore, it would be reasonable to predict that the average

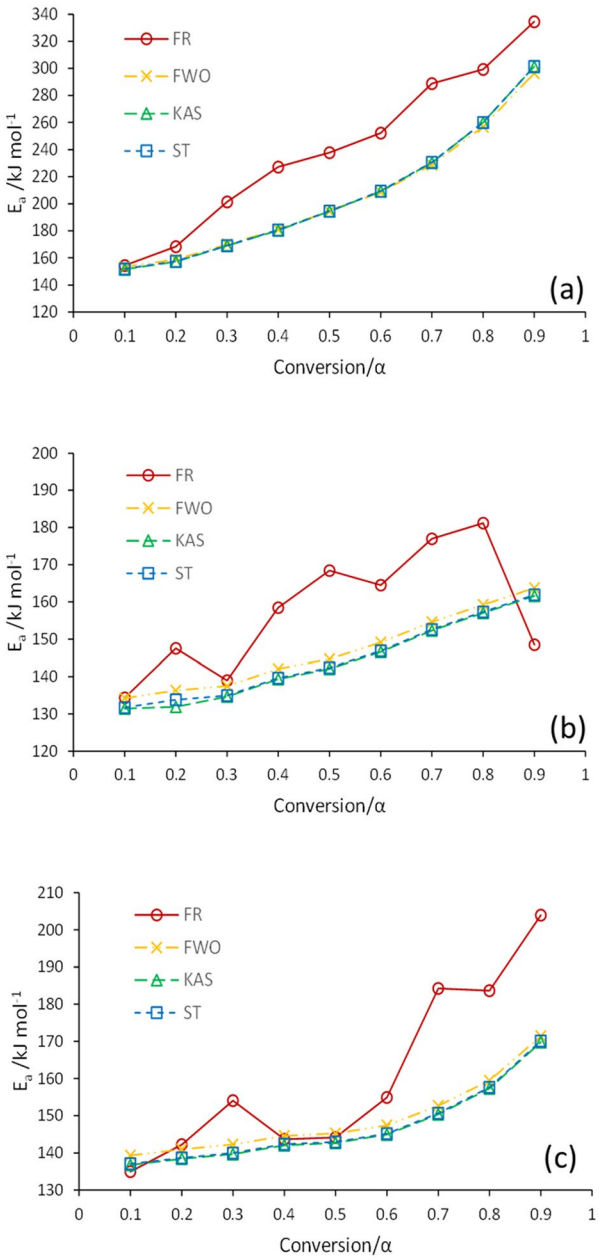

Fig. 4 E_a—α graphs generated for the particle sizes of **a** PCB-2, **b** PCB-3, **c** PCB-4

E_a values will not significantly change even at particle sizes smaller than the lowest particle size studied. It is worth to mention that the above mentioned result of current study does not coincide with the result of Chiang et al. [37] The pyrolysis of integrated circuit board was studied in a thermogravimetric system at four different particle sizes (4.0–4.8, 2.0–4.0, 1.0–2.0 and 0.42–1.0 mm) by Chiang et al., and they reported an insignificant difference in activation energy of main pyrolysis reaction for different particle sizes.

The kinetic parameter calculation results of the present study were compared with the results of previous similar studies in the literature. Chiang et al. [37] calculated the E_a values of main reaction for integrated circuit board pyrolysis at varying particle sizes as 192–197 kJ mol^{-1} and 160–169 kJ mol^{-1} for the heating rates of 2 and 15 °C min^{-1}, respectively, using the kinetic equation obtained by integrating Arrhenius equation and *n*th order reaction model to the Eq. (2) and taking its natural logarithm. They reported the reaction order as 1.24–1.47 and 1.23–1.58 for 2 and 15 °C min^{-1}. Quan et al. [15] studied the thermogravimetric pyrolysis of metal removed printed circuit board waste and calculated E_a values between 156.95 and 319.37 kJ mol^{-1} using distribution activation energy model. Hao et al. [38] carried out a thermogravimetric study including the pyrolysis of printed circuit board scraps and calculated the reaction order and E_a as 1.50 and 205 kJ mol^{-1}, respectively using CR method. Yao et al. [19] conducted the pyrolysis of non-metal fraction of waste printed circuit boards and calculated the average E_a values as 336.71, 329.66, 337.16, 337.07 and 341.93 kJ mol^{-1} using FR, FWO, ST, Tang and Boswell methods, respectively. They determined the reaction mechanism as F2 ($n=2$) using Criado method. Gao et al. [32] pyrolyzed non-metal fraction of waste printed circuit boards thermogravimetrically and calculated the E_a values as 173.60 and 172.62 kJ mol^{-1} using FWO and Kissinger methods, respectively. They also determined the kinetic mechanism function using Škvára-Šesták method as $g(\alpha)=(-\ln(1-\alpha))^2$ indicating a random nucleation followed by random growth model. Kim et al. [31] studied the pyrolysis of metal(copper)-free waste epoxy-printed circuit boards thermogravimetrically, and calculated the E_a value ranging from 141 to 582 kJ mol^{-1} with a mean value of 262 kJ mol^{-1} using revised Ozawa method. It can be said that the results of the literature studies mentioned up to this point and the present study are relatively conformable. However, it is worth to note that there are some other studies [34, 35, 39] in the literature in which E_a of PCBs were calculated at considerably low values (72.55–102.78 kJ mol^{-1}) compared to the present study. The difference observed for the E_a value may be due to the different feedstock properties and experimental conditions such as heating rate, particle size.

Evolved gas analysis

Two-dimensional (2D) infrared spectra were recorded during TG-FTIR analyses to detect the functional groups of evolved gas by pyrolysis of PCB-2, PCB-3 and PCB-4 samples at heating rate of 5 °C/min. 2D infrared spectra (Fig. 6) between 317 and 326 °C, where maximum mass loss rates occurred, were provided. As it can be seen in 2D FTIR spectra, 3621 cm^{-1} and 3575 cm^{-1} peaks associated with bromophenol and phenol, respectively. 3431 cm^{-1} peak showed the O–H bonds associated with H_2O. The double peaks were detected between 2500 cm^{-1} and 2250 cm^{-1} due to the

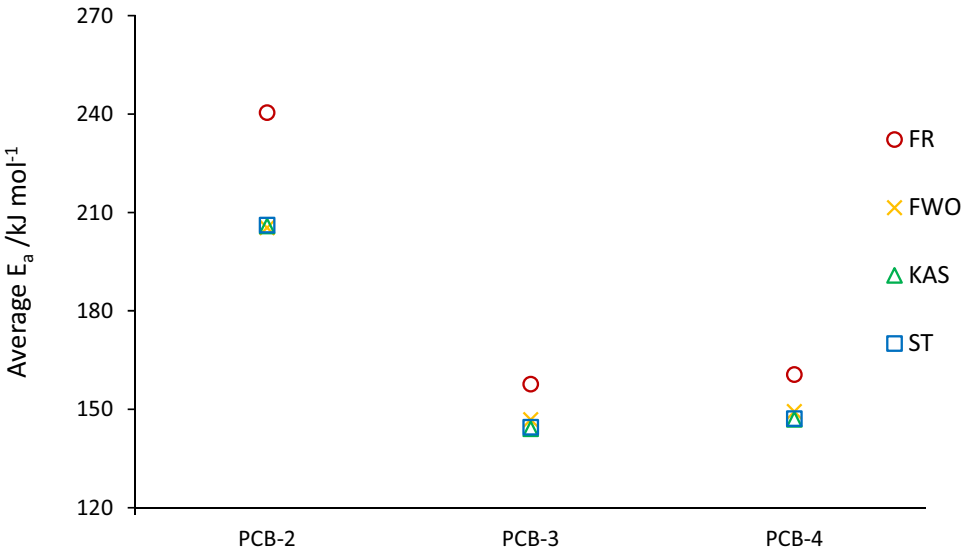

Fig. 5 Average E_a—particle size graphs generated for the studied kinetic methods

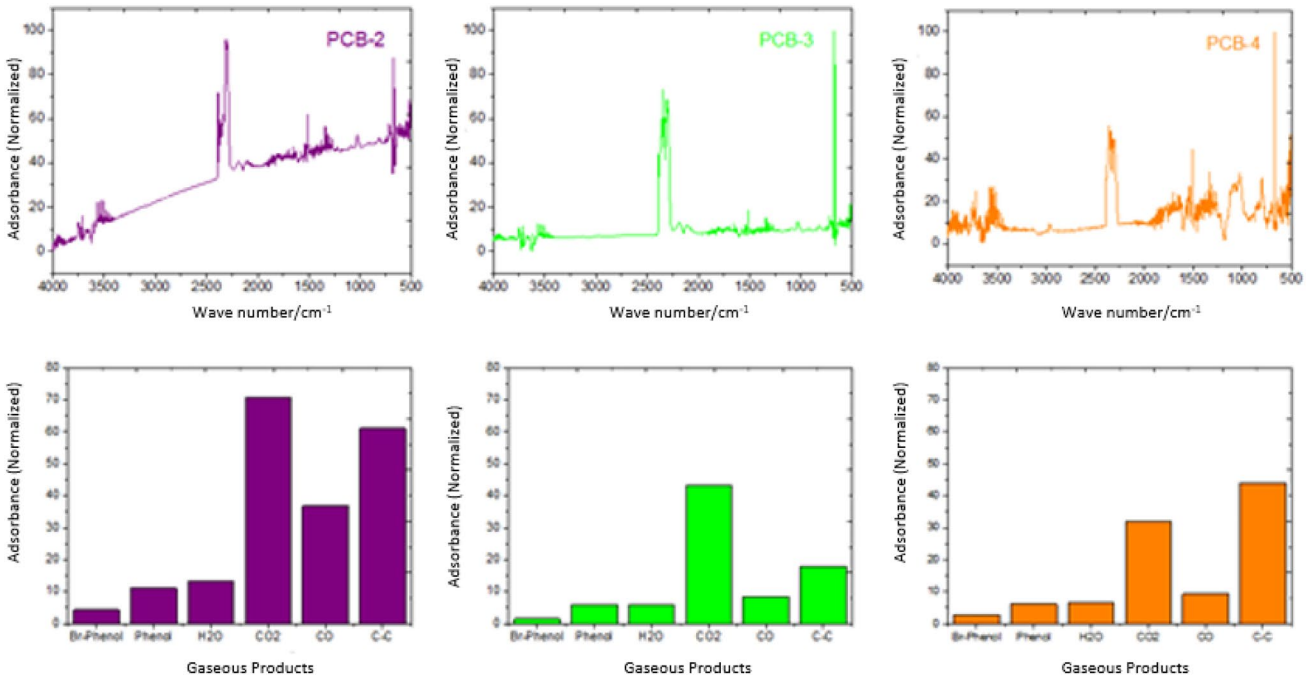

Fig. 6 The 2D infrared spectra of gas emissions evolved by pyrolysis of PCB wastes at 5 °C/min

asymmetric stretching vibration of CO_2 (2382 cm^{-1}) and CO (2144 cm^{-1}). In addition to this, 1510 cm^{-1} might indicate vibration of benzene functional group because of the stretching of carbon–carbon bonds of benzene rings. These results demonstrated some consistencies with the FTIR gas analysis results of other studies [40–42]. The presence of CO and CO_2 in pyrolysis gases is related to the presence of oxygen in the polymeric structure of PCB waste. Polycarbonates and epoxy resins in the polymeric structure of waste cards contain oxygen in their structure [28].

Figure 6 presents the absorbance values at specific wave numbers related to each gas evolved during the temperature range where the maximum decomposition rate of pyrolysis process took place. The peak with the highest absorbance of gas products during pyrolysis was CO_2, while the lowest peak belonged to bromophenol. According to the normalized absorbance values of each gaseous product given in Fig. 6, the order of the emission concentration of gas products for PCB-2 fraction can be acquired respectively as: $CO_2 > C–C > CO > H_2O >$ Phenol > Br-Phenol. A similar

order was also observed for the other fractions (i.e. PCB-3 and PCB-4) with an only exception that C–C concentration replaced with CO_2 and ranked first for PCB-4. CO_2 gas was observed at least in PCB-4 and at most in PCB 2. The reason for the highest CO_2 presence in PCB-2 might be due to higher polycarbonate and epoxy resin contents in this fraction [28]. Due to the presence of epoxy resins, the formation of phenol and phenol-derived components in the pyrolysis gas product at low temperatures, such as 300 °C, occurred in a small amount. This result coincides with the study conducted by Guo et al. [43].

Liquid phase analysis

Liquid produced from the pyrolysis of PCB-2 fraction were identified using GC/MS and the results are listed in SUB Table 2. The pyrolysis of PCB-2 generated large amounts of phenolic compounds, such as phenol (60%); phenol, 4-(1-methylethyl)- (11%); benzofuran, 2,3-dihydro-2-me (5%), phenol, 2-methyl-(5%), benzonitrile (5%) and phenol, 4-methyl- (3%). A similar composition of pyrolysis products has been reported in the literature and it is know that that 50% of the organic material in PCB wastes can be recovered as oil, which mainly consists of phenolic compounds [44]. In addition to this, bromine-bearing products such as benzenamine, 4-bromo-2,6-dim; phenol, 2-bromo- and benzene, 2-bromo-4-methyl-1- were also identified and the total content was calculated as 0.86% coming from the decomposition of brominated epoxy resin.

Conclusion

The characteristics, kinetic parameters and evolved gas analysis for pyrolysis of PCB wastes were studied thermogravimetrically on the basis of non-isothermal approach using a TG-FTIR analyser system. Studies revealed that the pyrolysis of PCB waste essentially started in the range of 285–315 °C, depending on the heating rate rather than the particle size, and after 541–565 °C, the mass loss rate was extremely low. The highest mass loss occurred in the range of 289–388 °C, i.e. main pyrolysis stage, depending on the particle size rather than the heating rate.

Kinetic parameters of main pyrolysis stage were calculated using Criado method, model-fitting CR method and isoconversional methods of FR, FWO, KAS and ST. The average E_a values calculated using all studied kinetic methods varied between 144.11 and 240.43 kJ mol^{-1}. The reaction mechanism was shown to fit type F2-2.5 for all the studied particle sizes and heating rates using CR and Criado methods. The average E_a values decreased by decreasing the particle size from PCB-2 to PCB-3, however, further decreasing of particle size from PCB-3 to PCB-4 did not affect the average E_a values according to the results obtained using isoconversional kinetic methods.

According to the evolved gas analysis results, CO_2 was released in all fractions due to the presence of epoxy resins and the formation of phenol and phenol-derived components in the pyrolysis gas product. The present study provides the information about pyrolysis behaviour, kinetics and evolved gases during the process necessary for the design, operation and optimization studies in the recycling of PCB wastes via pyrolysis process.

Supplementary Information The online version contains supplementary material available at https://doi.org/10.1007/s10163-023-01673-0.

Acknowledgements This work was supported by Yıldız Technical University Scientific Research Projects Coordinator's project numbered FBA-2021-4087.

Author contributions HHC: investigation, writing—original draft. KA: conceptualization, methodology, validation, formal analysis, writing—original draft, writing—review and editing, revision. AKF: conceptualization, resources, writing—review and editing, supervision, funding acquisition, revision.

References

1. dos Santos DM, Buzzi DC, Botelho Junior AB et al (2022) Recycling of printed circuit boards: ultrasound-assisted comminution and leaching for metals recovery. J Mater Cycles Waste Manag 24:1991–2001
2. Ghimire H, Ariya PA (2020) E-wastes: bridging the knowledge gaps in global production budgets, composition, recycling and sustainability implications. Sustain Chem 1(2):154–182
3. Du N, Ma H, Zhang H, Yang F, Li Z (2019) Simulation study on the heat transfer characteristics of a single printed circuit board particle in the pyrolysis process. Fuel Process Technol 192:45–56
4. Khanna R, Ikram-Ul-Haq M, Cayumil R, Rajarao R, Sahajwalla V (2015) Novel carbon micro fibers and foams from waste printed circuit boards. Fuel Process Technol 134:473–479
5. Stenvall E, Tostar S, Boldizar A, Foreman MRS, Möller K (2013) An analysis of the composition and metal contamination of plastics from waste electrical and electronic equipment (WEEE). Waste Manag 33:915–922
6. Tunali M, Tunali MM, Yenigun O (2021) Characterization of different types of electronic waste: heavy metal, precious metal and rare earth element content by comparing different digestıon methods. J Mater Cycles Waste Manag 23:149–157
7. Tuncuk A, Stazi V, Akcil A, Yazici EY, Deveci H (2012) Aqueous metal recovery techniques from e-scrap: hydrometallurgy in recycling. Miner Eng 25:28–37
8. Jie G, Ying-Shun L, Mai-Xi L (2008) Product characterization of waste printed circuit board by pyrolysis. J Anal Appl Pyrolysis 83(2):185–189
9. Hao J, Wang H, Chen S, Cai B, Ge L, Xia W (2014) Pyrolysis characteristics of the mixture of printed circuit board scraps and coal powder. Waste Manag 34(10):1763–1769
10. Utetiwabo W, Yang L, Tufail MK, Zhou L, Chen R, Lian Y et al (2020) Electrode materials derived from plastic wastes and other industrial wastes for supercapacitors. Chin Chem Lett 31(6):1474–1489

11. Liu W, Xu J, Han J, Jiao F, Qin W, Li Z (2019) Kinetic and mechanism studies on pyrolysis of printed circuit boards in the absence and presence of copper. ACS Sustain Chem Eng 7(2):1879–1889
12. Alenezi RA, Al-Fadhli FM (2018) Thermal degradation kinetics of waste printed circuit boards. Chem Eng Res Des 130:87–94
13. Evangelopoulos P, Kantarelis E, Yang W (2017) Experimental investigation of printed circuit boards for energy and materials recovery under nitrogen and steam atmosphere. Energy Procedia 105:986–991
14. Zhan Z, Qiu K (2011) Pyrolysis kinetics and TG-FTIR analysis of waste epoxy printed circuit boards. J Cent South Univ Technol 18:331–336
15. Quan C, Li A, Gao N (2009) Thermogravimetric analysis and kinetic study on large particles of printed circuit board wastes. Waste Manag 29:2353–2360
16. Soria-Verdugo A, Morgano MT, Mätzing H, Goos E, Leibold H, Merz D, Riedel U, Stapf D (2020) Comparison of wood pyrolysis kinetics data derived from thermogravimetric experiments by model-fitting and model-free methods. Energy Convers Manag 212:112818
17. Miura K (2002) A new and simple method to estimate f(E) and k0(E) in the distributed activation energy model from three sets of experimental data. Energy Fuels 9(2):302–307
18. Sun J, Wang W, Liu Z, Ma Q, Zhao C, Ma C (2012) Kinetic study of the pyrolysis of waste printed circuit boards subject to conventional and microwave heating. Energies 5:3295–3306
19. Yao Z, Xiong J, Yu S, Su W, Wu W, Tang J, Wu D (2020) Kinetic study on the slow pyrolysis of non-metal fraction of waste printed circuit boards (NMF-WPCBs). Waste Manag Res 38(8):903–910
20. Tao R, Xing P, Li H, Cun Z, Wang C, Ma S, Sun Z (2023) Kinetics study and recycling strategies in different stages of full-component pyrolysis of spent $LiNixCoyMnzO_2$ lithium-ion batteries. Waste Manag 155:8–18
21. Ali L, Mousa HA, Al-Harahsheh M, Al-Zuhair S, Abu-Jdayil B, Al-Marzouqi M, Altarawneh M (2022) Removal of bromine from the non-metallic fraction in printed circuit board via its co-pyrolysis with alumina. Waste Manag 137:283–293
22. Açıkalın K (2021) Determination of kinetic triplet, thermal degradation behaviour and thermodynamic properties for pyrolysis of a lignocellulosic biomass. Bioresour Technol 337:125438
23. Jiang Q, Wang H, Liu J et al (2022) Nonisothermal pyrolysis kinetics of waste printed circuit boards and product characterization using TG–MS. J Mater Cycles Waste Manag 24:2151–2161
24. Sun Y, Zhang H, Zhang F, Tao J, Cheng Z, Yan B, Chen G (2022) Pyrolysis properties and kinetics of photocured waste from photopolymerization-based 3D printing: a TG-FTIR/GC–MS study. Waste Manag 150:151–160
25. Mao R, Shao J, Wang G, Wang F, Wang C (2022) Thermal behavior and kinetics analysis of co-combustion of petroleum coke and paper sludge-derived hydrochar. Waste Manag 153:405–414
26. Singh V, Srivastava VC (2022) Insight into the thermal kinetics and thermodynamics of sulfuric acid plant sludge for efficient recovery of sulphur. Waste Manag 140:233–244
27. Zhang Z, Xu G, Wang Q, Cui Z, Wang L (2019) Pyrolysis characteristics, kinetics, and evolved gas determination of chrome-tanned sludge by thermogravimetry–Fourier-transform infrared spectroscopy and pyrolysis gas chromatography-mass spectrometry. Waste Manag 93:103–137
28. Marco I, Caballero BM, Chomón MJ, Laresgoiti MF, Torres A, Fernández G, Arnaiz S (2008) Pyrolysis of electrical and electronic wastes. J Anal Appl Pyrolysis 82:179–183
29. Szalatkiewicz J (2014) Metal content in printed circuit board waste. Pol J Environ Stud 23(6):2365–2369
30. Li J, Duan H, Yu K, Liu L, Wang S (2010) Characteristic of low-temperature pyrolysis of printed circuit boards subjected to various atmosphere. Resour Conserv Recycl 54:810–815
31. Kim YM, Kim S, Lee JY, Park YK (2013) Pyrolysis reaction pathways of waste epoxy-printed circuit board. Environ Eng Sci 30(11):706–712
32. Gao R, Zhan L, Guo J, Xu Z (2020) Research of the thermal decomposition mechanism and pyrolysis pathways from macromonomer to small molecule of waste printed circuit board. J Hazard Mater 383:121234
33. Yousef S, Elmontas J, Striūgas N, Zakarauskas K, Praspaliauskas M, Abdelnaby MA (2020) Pyrolysis kinetic behaviour and TG-FTIR-GC-MS analysis of metallised food packaging plastics. Fuel 282:118737
34. Hong L, Wang B, Zhou Q (2014) Thermogravimetric analysis and kinetic study of waste printed circuit board in various atmospheres. Adv Mater Res 864–867:1929–1932
35. Ng CH, Salmiaton A, Hizam H (2014) Catalytic pyrolysis and a pyrolysis kinetic study of shredded printed circuit board for fuel recovery. Bull Chem React Eng Catal 9(3):224–240
36. Vyazovkin S, Burnham AK, Criado JM, Pérez-Maqueda LA, Popescu C, Sbirrazzuoli N (2011) ICTAC Kinetics Committee recommendations for performing kinetic computations on thermal analysis data. Thermochim Acta 520:1–19
37. Chiang HL, Lin KH, Lai MH, Chen TC, Ma SY (2007) Pyrolysis characteristics of integrated circuit boards at various particle sizes and temperature. J Hazard Mater 149:151–159
38. Hao J, Wang H, Chen S, Cai B, Ge L, Xia W (2014) Pyrolysis characteristics of the mixture of printed circuit board scraps and coal powder. Waste Manag 34:1763–1769
39. Kantarelis E, Yang W, Blasiak W, Forsgren C, Zabaniotou A (2011) Thermochemical treatment of E-waste from small household appliances using highly pre-heated nitrogen-thermogravimetric investigation and pyrolysis kinetics. Appl Energy 88:922–929
40. Sahajwalla V, Cayumil R, Khanna R, Ikram-Ul-Haq M, Rajarao R, Mukherjee PS, Hill A (2015) Recycling polymer-rich waste printed circuit boards at high temperatures: recovery of value-added carbon resources. J Sustain Metall 1:75–84
41. Quan C, Li A, Gao N (2012) Research on pyrolsis of PCB waste with TG-FTIR and Py-GC/MS. J Therm Anal Calorim 110:1463–1470
42. Bi H, Wang C, Lin Q, Jiang X, Jiang C, Bao L (2021) Pyrolysis characteristics, artificial neural network modeling and environmental impact of coal gangue and biomass by TG-FTIR. Sci Total Environ 751:142293
43. Guo Q, Yue X, Wang M, Liu Y (2010) Pyrolysis of scrap printed circuit board plastic particles in a fluidized bed. Powder Technol 198(3):422
44. Ma C, Kumagai S, Saito Y, Kameda T, Yoshioka T (2021) Enhanced production of phenol and debromination by co-pyrolysis of the non-metallic fraction of printed circuit boards and waste tires. Green Chem 23(17):6392–6404